Spray deposition of $AgBiS_2$ and Cu_3BiS_3 thin films for photovoltaic applications

Received 00th January 20xx,
Accepted 00th January 20xx

DOI: 10.1039/x0xx00000x

www.rsc.org/

Narendra Pai[a], Jianfeng Lu[a], Dimuthu C. Senevirathna[a], Anthony S. R. Chesman[b], Thomas Gengenbach[b], Manjunath Chatti[ac], Udo Bach[b,d,e], Philip C. Andrews[a], Leone Spiccia[a,c,⊥], Yi-Bing Cheng[f,g,*], and Alexandr N. Simonov[a,c,*]

Spray pyrolysis of bismuth(III) tris(4-methylbenzodithioate) toluene solutions containing either silver(I) acetate and 1-octanethiol, or copper(I) acetate and 1,2-ethane dithiol is introduced as a low-temperature solution-based method to produce sub-100 nm thick coatings of α cubic rock salt $AgBiS_2$ and orthorhombic Cu_3BiS_3. The structure, morphology and optoelectronic properties of the materials thus obtained have been comprehensively characterised using conventional techniques. Extensive optimisation of the deposition conditions has been undertaken to achieve the formation of uniform, 60–70 nm thick films of densely packed $AgBiS_2$ and Cu_3BiS_3 crystallites with a typical size of 10–20 nm. Planar photovoltaic devices based on spray-deposited $AgBiS_2$ as a light harvester, ZnO as an electron transporting layer, and spiro-OMeTAD as a hole transporting material produce short-circuit current densities as high as 18.1 ± 0.6 mA cm^{-2} under 1 sun AM1.5G irradiation. The devices are stable without encapsulation under ambient conditions for at least 1 month.

Introduction

Chalcogenides have come to the forefront of the science of functional materials as a class of versatile compounds with tunable and often unique thermoelectric, (photo)(electro)catalytic and optoelectronic properties.[1-4] Different types of chalcogenides have carved niches in a range of applications that include nonlinear optics,[5] light emitting *in vivo* bioimaging,[6] energy storage,[7, 8] electrocatalysis[3, 9] and photovoltaics.[4, 8] Till now, binary metal chalcogenides containing either noxious lead and cadmium, or scarce elements like tellurium and indium have dominated research in the aforementioned areas, eventuating in commercialisation in the most successful cases.[10-13] However, increasingly strict ecological regulations and the urge towards development of cheaper and safer materials have promoted continuously enhancing interest in ternary chalcogenides based on non-toxic and environmentally friendly elements.[1] From this perspective, bismuth-based systems are particularly attractive as solution-processable materials with a range of useful physical and chemical properties.[14,15]

Among non-toxic ternary chalcogenides currently considered for applications in photovoltaics, silver bismuth disulphide ($AgBiS_2$) stands out as a promising photoconductive material with intrinsic stoichiometric stability.[16] It has already been applied in solar cells both as a counter electrode[17] and as a light-absorber.[18, 19] In the latter case, a comparatively high absorption coefficient (10^5 to 10^3 cm^{-1} within the 400–1100 nm wavelength range) of the stable α cubic rock salt $AgBiS_2$ phase (formed at *ca* 473 K)[15, 20] enables promising photovoltaic performance as recently reported by Bernechea *et al*.[21] for very thin layers of this chalcogenide sandwiched between electron- and hole-conducting materials. Another prospective ternary bismuth chalcogenide for optoelectronic applications is Cu_3BiS_3, which exhibits an orthorhombic crystal structure, *p*-type conductivity, and an impressive absorption coefficient of approximately 10^5 cm^{-1} in the visible region.[22]

Vacuum fusing[23] and flux techniques[24] were the most commonly applied methods to synthesise $AgBiS_2$ until Chen *et al.* established polyol and microwave-assisted routes as significantly less resource intensive procedures to obtain silver-bismuth disulphide rods and dendrites.[25, 26] Later, Thongtem *et al.* demonstrated the synthesis of $AgBiS_2$ nanostructured "flowers" *via* low-temperature solvothermal and cyclic microwave techniques.[27, 28] Most recently, Bernechea *et al*. introduced a hot-injection method to produce ligand-stabilised cubic phase $AgBiS_2$ particles that are only several nm in size.[19] Importantly, the above synthetic protocols eliminate the requirement to use metallic silver and bismuth along with sulphur powder as the starting materials,[15, 26] which is a critical advantage over the high-temperature flux methods. Instead, the solution processable precursors like bismuth and silver nitrates or acetates,[29] thiourea,[25] thiosemicarbazide,[27] L-cysteine,[30] hexamethyldisilathiane[19] or Na_2S[18] can be employed. Cu_3BiS_3 in a variety of morphologies can be synthesised *via* a range of physical and chemical techniques, such as sputtering,[31] thermal evaporation,[32] spray pyrolysis,[33] spin coating[34] and chemical bath deposition.[35] In a recent report from some of us, bismuth(III) aryldithioates were introduced as a new type of precursor for both bismuth and sulphur that can be combined with soluble Ag^I or Cu^I salts to produce $AgBiS_2$ and Cu_3BiS_3 nanoparticles, respectively, upon mild microwave treatment.[36]

The above reports have significantly broadened the possibilities to prepare small particles of silver and copper bismuth

[a] School of Chemistry, Monash University, Melbourne, Victoria, 3800, Australia
[b] Commonwealth Scientific and Industrial Research Organisation Manufacturing, Clayton, Victoria 3168, Australia
[c] ARC Centre of Excellence for Electromaterials Science, Monash University, Melbourne, Victoria, 3800, Australia
[d] ARC Centre of Excellence in Exciton Science and Department of Chemical Engineering, Monash University, Melbourne, Victoria, 3800, Australia
[e] The Melbourne Centre for Nanofabrication, Clayton, Victoria 3168, Australia
[f] ARC Centre of Excellence in Exciton Science and Department of Materials Science and Engineering, Monash University, Melbourne, Victoria, 3800, Australia
[g] State Key Laboratory of Advanced Technology for Materials Synthesis and Processing, Wuhan University of Technology, Wuhan 430070, China

Electronic Supplementary Information (ESI) available: NMR and IR spectra; XP spectra; TEM images; SAED pattern; TGA data; PESA and UPS plots, J-V curves; summary of photovoltaic parameters; stability data.
See DOI: 10.1039/x0xx00000x

sulphides. However, less success has been achieved hitherto in the fabrication of thin homogeneous $AgBiS_2$ and Cu_3BiS_3 films, as needed for optoelectronic applications. Indeed, given that no intrinsic photogenerated charge-separation mechanism exists in ternary bismuth-based sulphides and the charge diffusion lengths are comparatively short,[16] a planar configuration for optoelectronic devices, and in particular photovoltaic devices with a very thin light-absorber layer, is seen as the most advantageous architecture. Reported strategies to deposit $AgBiS_2$ as a film are predominantly based either on direct thermal evaporation of the compound,[38] or sonochemical approach,[37] or casting layers of a pre-formed $AgBiS_2$ particles.[17, 19] The high-temperature evaporation and similar gas-to-particle deposition methods have obvious technological disadvantages, which include the use of sophisticated instrumentation, comparatively low productivity, and overall high cost. With the particle pre-forming/deposition approach, the formation of homogeneous and pin-hole-free layers where small crystallites are densely packed and interconnected is typically hard to achieve. Overall, fabrication of uniform, stable and thin $AgBiS_2$ layers under mild conditions is yet challenging, and development of an easy-to-scale, highly reproducible and low-cost method is needed to facilitate integration of this chalcogenide material into optoelectronic devices.

One robust and rapid deposition technique that has not been applied for the synthesis of $AgBiS_2$ previously is spray pyrolysis. Considering the simplicity of the apparatus and its high productivity, this versatile method is technologically attractive for the production of thin films with facile control over thickness.[39] Importantly, the procedure does not require the use of vacuum or very high temperatures at any stage. Cu_3BiS_3 has been successfully deposited as 250–300 nm thick films onto glass[33] *via* spray pyrolysis of solutions containing $BiCl_3$, $CuCl_2$ and thiourea. However, the uniformity and morphological homogeneity of the resulting coatings would require significant improvements if integration into optoelectronic devices is pursued. Besides, thinner films could not be obtained by using the reported method.

The present work reports on the spray pyrolysis deposition of ternary $AgBiS_2$ semiconductor films with controllable, sub-100-nm thickness using dual-source bismuth 4-methyl benzodithiolate and silver acetate as precursors. The deposition conditions have been optimised to enhance the photovoltaic effect for the fabricated films when integrated into planar configuration solar cells, and a comprehensive physical characterisation of the produced materials and photovoltaic devices has been undertaken. The possibility to deposit Cu_3BiS_3 thin films following the same strategy is also demonstrated.

Experimental

Materials

All chemicals were purchased from Sigma-Aldrich and used as received from suppliers without any further purification unless otherwise stated. 2,2′,7,7′-tetrakis (N,N-di-p-methoxy phenylamino)-9,9 spirobifluorene (Spiro-OMeTAD) was obtained from *Luminescence Technology Corp*. PTB7 (poly[(4,8-bis-(2-ethylhexyloxy)-benzo(1,2-b:4,5-b′)dithiophene)-2,6-diyl-alt-(4-(2-ethylhexyl)-3-fluorothieno[3,4-b]thiophene-)-2 carboxylate -2-6-diyl)]) was purchased from *1-Material*. P3HT (poly(3-hexylthiophene-2,5-diyl) was purchased from *Rieke Metals*. $Co(bpyPY4)](OTf)_{2.66}$ (cobalt(II,III) 6,6'-bis(1,1-di(pyridin-2-yl)ethyl)-2,2'-bipyridine triflate) was synthesised as reported in Ref.[40] Bismuth tris(4-methylbenzodithioate) [$Bi(4\text{-}MBDT)_3$] was synthesised *via* a sonochemical reaction of bismite (Bi_2O_3) with 4-methylbenzodithioic acid (4-MBDT) in toluene followed by filtration and recrystallisation in hot toluene as reported previously.[41] The composition and structure were confirmed by elemental analysis, mass-, ^{1}H- and ^{13}C-NMR spectroscopy (Figure S1).

Substrate preparation

Glass sheets (10 cm × 10 cm) coated with indium tin oxide (ITO) with a sheet resistance of *ca* 15 Ω sq^{-1} were purchased from *Lumtec* and used as substrates for thin film deposition. The ITO substrates were cleaned by ultrasonication in 2% Helmanex surfactant aqueous solution, acetone and isopropanol (15 min in each medium), dried under N_2 flow, and plasma treated at 1000 mTorr for 15 min (*Harrick Plasma* cleaner). Laser patterned substrates were then cut into smaller pieces of the dimensions 2.5 cm × 2.5 cm and a ZnO layer was deposited by spin-coating (3000 rpm; 30 s) 30 uL of the precursor solution (1 g of zinc acetate dehydrate and 284 µL ethanolamine in 10 ml methoxyethanol) and subsequent heating at 200 °C for 30 min on air. Two spin-coating/annealing cycles were applied to achieve a ZnO thickness of *ca* 45 nm.

Spray pyrolysis deposition

The precursor solution for $AgBiS_2$ was prepared as follows: bismuth(III) *tris*(4-methylbenzodithioate) (23.10 mg) was dissolved in 8 ml toluene at 50 °C; silver acetate (5.34 mg) and 1-octanethiol (0.55 mL) were then added to the solution under vigorous stirring, which was continued for one hour at 50 °C. The precursor solution for Cu_3BiS_3 was prepared by adding 11.8 mg copper(I) acetate with 0.34 mL 1,2-ethanedithiol to bismuth(III) *tris*(*4*-methylbenzodithioate) toluene solution (the same concentration as for $AgBiS_2$ precursor). Thus prepared solutions were then immediately employed for spray pyrolysis onto 2.5 cm × 2.5 cm ZnO|ITO substrates using a spray nozzle (*Glass Keller*, Falcon sprayer with borosilicate glass 19/26 15 mL capacity glass tube) connected to compressed air (18×10^5 Pa). The substrates were maintained at a defined temperature (100–250 °C) provided by a Harry Gestigkeit GmbH titanium hotplate during deposition and for additional 30 min after spraying was complete. The optimised spray conditions were as follows: 4 mM bismuth and 4 mM silver precursor concentrations with 40 mM 1-octanethiol or 4 mM bismuth and 12 mM copper precursor concentrations with 50 mM 1,2-ethanedithiol (excess thiols were necessary to compensate for sulphur loss during thermal deposition), sprayed solution volume - 7 mL, nozzle to substrate distance - 12 cm, intermittent cycles with 0.5 s continuous spraying and 20 seconds wait time. The number of deposition cycles was varied as discussed in the text below. All of the above procedures were carried out in air,

though inside a fume hood to provide fast removal of gaseous products and solvent vapors. The films were allowed to cool to ambient temperature (24 ± 2 °C) naturally.

Photovoltaic device fabrication

2.5 cm × 2.5 cm $AgBiS_2$|ZnO|ITO and Cu_3BiS_3|ZnO|ITO samples were further transferred into a N_2-filled glovebox and modified with a hole-transporting material (HTM) layer (Spiro-OMeTAD, PTB7, P3HT, $[Co(bpyPY4)](OTf)_{2.66}$, CuSCN or CuI), a back-contact (Ag) and a mask to complete a photovoltaic device. Spiro-OMeTAD was deposited by spin-coating (3000 rpm, 30 s) 25 µL of the chlorobenzene solution containing 60 mM HTM, 32 mM lithium bis(trifluoromethanesulfonyl)imide (LiTFSI), 200 mM tert-butylpyridine (tBP) and 1.8 mM bis(2,6-di(1H-pyrazol-1-yl)pyridine) cobalt(II) di[bis(trifluoromethane) sulfonimide] (FK269). Dichlorobenzene solutions of PTB7 (5 mg mL^{-1}) and P3HT (20 mg mL^{-1}) were spin-coated at 2000 rpm for 30 s. In some cases, MoO_3 (nominal thickness 5 nm) was thermally evaporated onto the above HTM layers. CuSCN and CuI layers were obtained by spin-coating (2000 rpm, 30 s) 1 ml of their diethyl sulphide solutions (30 mg of CuSCN; 20 mg of CuI) followed by heating at 60 °C for 10 min. $[Co(bpyPY4)](OTf)_{2.66}$ deposition solution was prepared by mixing solutions of $[Co^{III}(bpyPY4)](OTf)_3$ (26.7 mg in 1 ml nitromethane) and $[Co^{II}(bpyPY4)](OTf)_2$ (24.6 mg in 1 ml nitromethane) in 2:1 ratio (120:60 uL) with 1.12 uL LiTFSI (520 mg mL^{-1}) and 2.52 uL tBP; 40 uL of this solution was spin-coated at 2500 rpm for 40 sec. On top of a HTM later, a 120-nm-thick silver back contact was evaporated (DDong DD-GCMO3CR; initial vacuum level 8×10^{-6} Torr). Photomask was finally applied to produce solar cells with an active area of 0.16 or 1.00 cm^2.

Characterisation

X-ray diffraction patterns were obtained using a D2 Advance BRUKER diffractometer with Cu-K_α radiation (λ = 1.5406 Å) source operating at 30 kV and 15 mA at a scan rate of 0.5° min^{-1}. Spray-deposited $AgBiS_2$ and Cu_3BiS_3 films with 100 nm thickness were used for the analysis.

X-ray photoelectron spectroscopic (XPS) analysis was performed with an AXIS Nova spectrometer (*Kratos Analytical Inc.*) at about 1×10^{-8} mbar with a monochromatic Al-K_α X-ray source operating at a power of 180 W (15 kV × 12 mA) and a hemispherical analyser in fixed analyser transmission mode. High resolution spectra were recorded at pass energy of 40 eV with an overall spectral resolution of better than 0.9 eV. The accuracy associated with quantitative analysis in XPS is generally considered to be 10 – 15 %. 100-nm thick films of $AgBiS_2$ spray-coated onto 2 cm × 2 cm ITO substrates were used for XPS analysis.

Fourier transformed infrared (FTIR) spectra were recorded with an Agilent Technologies Cary 630 spectrometer. Bismuth(III) *tris*(*4*-methylbenzodithioate) crystals and silver dodecyl thiolate were dissolved in toluene and then dried on a rotary evaporator to produce a "precursor" sample. $AgBiS_2$ was deposited by spray-pyrolysis onto glass substrates and scratched for analysis.

Differential scanning calorimetry was carried for the dried $AgBiS_2$ samples in 70 µL alumina pans within the 25-800 °C temperature range (heating rate 4 °C min^{-1}) in dinitrogen atmosphere using Mettler Toledo TGA/DSC 1 star system.

Scanning electron micrographs (SEM) in a secondary and backscattered electron detection modes were obtained with a FEI Nova NanoSEM 450 microscope at a voltage of 5 kV and spot size of 2.5. The $AgBiS_2$ and Cu_3BiS_3 films deposited on ITO were immobilised on a specimen stub using double sided carbon tape. All samples were coated with a *ca* 1 nm layer of iridium to minimise charging effects. Local energy dispersive X-ray elemental analysis was provided by Bruker Quantax 400 X-ray detector.

Transmission electron microscopic (TEM) analysis was undertaken on an FEI Tecnai T20 microscope operating at an accelerating voltage of 200 kV. Samples were prepared by drop-casting a dispersion of $AgBiS_2$ in ethanol on a holey carbon 300 mesh Cu grid.

UV–Vis-NIR spectra of spray-deposited $AgBiS_2$ and Cu_3BiS_3 films were recorded in transmission and reflectance modes using a PerkinElmer Lambda 1050 spectrophotometer equipped with an integrating sphere. Bare glass substrate was used to obtain background spectra. Absorption coefficient, $\alpha(\lambda)$, of the films was derived from the equation:[42]

$$a(\lambda) = \frac{1}{t}\ln\left[\left(\frac{(1-R(\lambda))^2}{2T(\lambda)}\right) + \sqrt{\left(\frac{(1-R(\lambda))^4}{4T(\lambda)^2}\right) + R(\lambda)^2}\right],$$

where, t is film thickness, $T(\lambda)$ and $R(\lambda)$ are background-corrected transmittance and reflectance, respectively. **Photoelectron Spectroscopy in Air (PESA)** measurements were undertaken using a Riken Kekei AC-2 spectrometer in a power intensity range from 20 to 50 nW. 100-nm thick films of $AgBiS_2$ or Cu_3BiS_3 spray coated onto 2 cm × 2 cm glass substrates were used for analysis.

Ultraviolet photoelectron spectroscopic (UPS) analysis was performed using an AXIS Ultra DLD spectrometer (*Kratos Analytical Inc.*) at about 1×10^{-8} mbar with a He discharge lamp producing He I UV radiation (incident photon energy: 21.22 eV), a hemispherical analyser operating in fixed analyser transmission mode and a standard aperture (analysis area: 0.3 mm × 0.7 mm). Samples were biased at –9 V to facilitate measuring the secondary electron cut-off. Spectra were recorded at a pass energy of 5 eV with a spectral resolution of better than 100 meV. Samples were prepared by spray depositing an appropriate precursor solution onto ITO substrates.

Photovoltaic characterisation was performed using a Keithley 2400 Source Meter under irradiation provided by an Oriel solar simulator fitted with a filtered 1000 W xenon lamp to replicate the AM 1.5 G spectrum. Unless otherwise stated, the light intensity was 100 mW cm^{-2} (1 sun) as calibrated using a silicon reference cell having a KG3 glass filter (*PV Measurements, Inc.*) with a black non-reflective metal mask to confine the area exposed to light to 0.16 cm^2. A Keithley 2400 Source Meter and a 300 W xenon lamp equipped with an Oriel Corner-stone 260 monochromator was used to record incident photon to current conversion efficiency (IPCE) spectra. A calibrated silicon cell (*Peccell Technologies*) was used to quantify the monochromatic photon flux.

Results and Discussion

Reaction of 4-methyldithiobenzenoic acid (4-MBDT) with bismuth oxide in toluene produces bismuth *tris*(4-methylbenzodithioate) [Bi(4-MBDT)$_3$], which is red in colour (Figure 1a) and highly crystalline, as reported by some of us elsewhere.[36, 41] Outcomes of the NMR and FTIR analyses of this material (Figure S1 and S2) were also in keeping with previous publications.[36, 41] Addition of silver acetate and 1-octane thiol to [Bi(4-MBDT)$_3$] dissolved in hot toluene forms a black homogeneous solution of AgBiL$^y_2$, where L^y denotes a mixed alkyl-arylthiolate ligand. Spray deposition followed by annealing in air at 125 ≤ *T* ≤ 200 °C of thus prepared AgBiL$^y_2$ toluene solution yields highly-dispersed $AgBiS_2$ particles (Figure 1a and Figure S3). This strategy allows for formation of uniform silver bismuth disulphide films with easily controlled thickness (Figure 1b). The composition of the sprayed precursor solution and instrumental spray parameters (see experimental for details) were optimised to provide the highest quality of the resulting $AgBiS_2$ films in terms of homogeneity and photovoltaic properties (*vide infra*), and were kept unchanged for all materials described further in the text. As will be also demonstrated below, replacing silver(I) acetate for copper(I) acetate and 1-octane thiol for 1,2-ethane dithiol in the precursor solution enables the deposition of thin homogeneous Cu_3BiS_3 films.

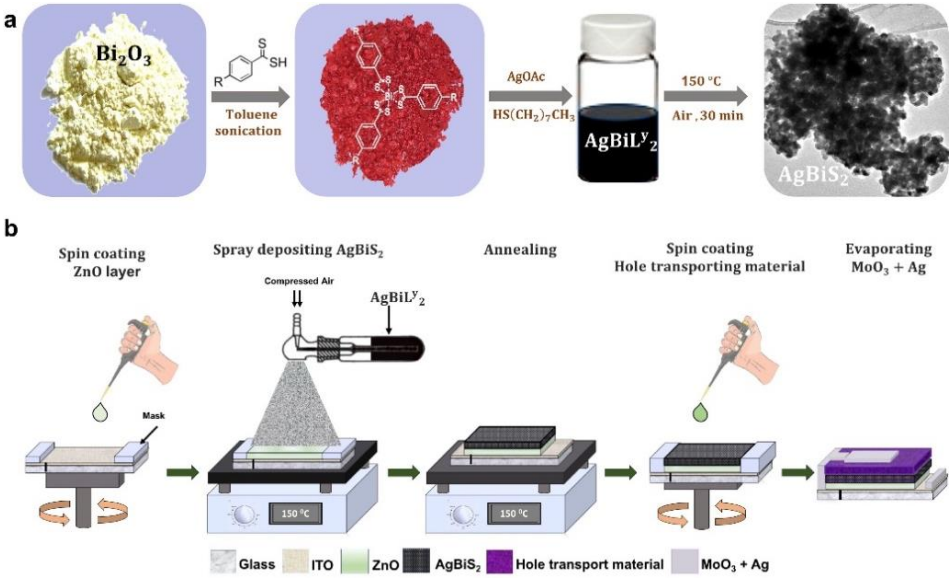

Figure 1. Schematic summary of (a) synthesis of $AgBiS_2$ nanoparticles, and (b) spray deposition of $AgBiS_2$ films and photovoltaic device fabrication.

Composition and morphology of $AgBiS_2$ films

Fast and quantitative conversion of the AgBiL$^y_2$ precursor to $AgBiS_2$ under employed spray conditions (Figure 1b and experimental) was confirmed by X-ray diffraction (Figure 2a) and FTIR spectroscopy (Figure S2). XRD patterns of the films deposited within the temperature interval 125 ≤ *T* ≤ 200 °C were consistent with the *α* cubic $AgBiS_2$ phase (JCPDS Card File No. 01-089-2045). No indications of the presence of Ag_2S, Bi_2S_3 or other undesired phases were identified by XRD (broad halo within the 2θ range 12–36° in diffractograms shown in Figure 2a is due to the ITO support). Equally importantly, attenuated total reflection FTIR analysis confirmed essentially complete removal of the methylbenzodithiolate ligand and octane thiol (Figure S2). Differential scanning calorimetry and thermogravimetric analysis undertaken under argon atmosphere for spray-deposited $AgBiS_2$ showed a relatively low mass loss of 1.5 % and an associated rise in heat flow within the temperature range 300–600 °C, which was tentatively attributed to the removal of residues of the organic compounds (Figure S4). It was also found that decomposition of $AgBiS_2$

under inert atmosphere commences at approximately 700 °C. TEM analysis of the freshly spray-deposited $AgBiS_2$ material that was scratched from the support surface revealed that the films are comprised of interconnected nanoparticles that are close to spherical in shape (Figure S3). Such morphology is most probably provided by the capping effect of octanethiol on the thiophilic bismuth-based surface, which suppresses the growth of the particles. When synthesis was undertaken at 150 °C, an average linear particle size of 12 ± 5 nm and a mean mass-weighed particle size of 16 nm were obtained (Figure S3b), though it is noted that the interconnected morphology introduces a reasonable level of uncertainty into these values.

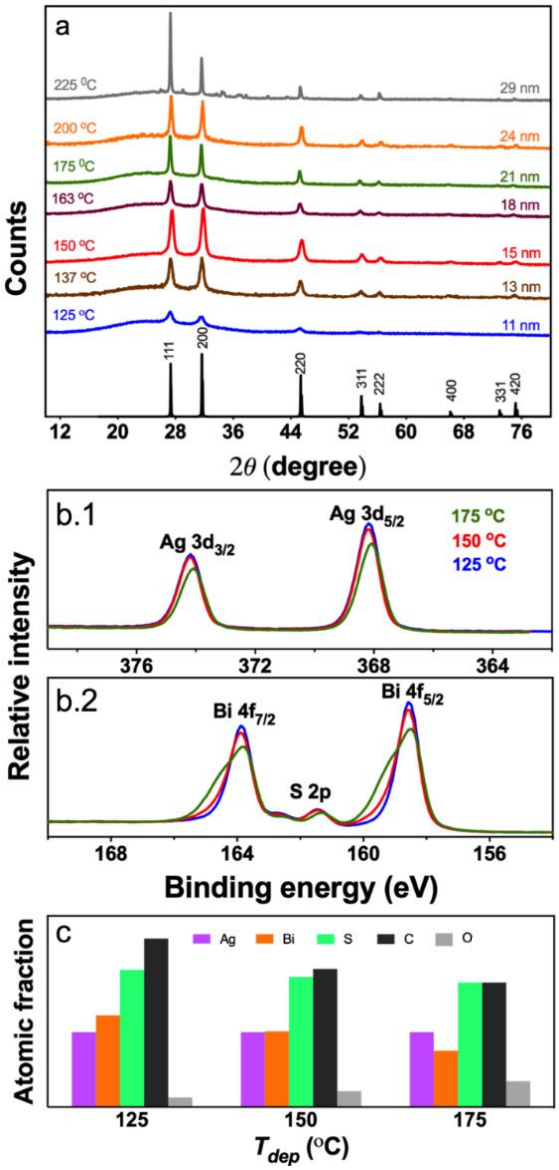

Figure 2. (a) XRD patterns, (b.1) Ag 3d, (b.2) Bi 4f and S 2p high resolution spectra for $AgBiS_2$ films formed by spray-pyrolysis on a flat glass support at different temperatures: *blue* – 125 °C; *brown* – 137 °C; *red* – 150 °C; *vine* – 163 °C; *green* – 175 °C; *orange* – 200 °C; *grey* – 225 °C. *Black* lines in panel **a** show reference reflections for cubic $AgBiS_2$ (JCPDS Card File No. 01-089-2045). Panel **c** shows relative surface concentrations of Ag, Bi, S, C, and O derived from the XPS data for the films obtained at 125, 150 and 175 °C (survey XP spectrum is shown in Figure S5).

Further, systematic examination of the effect of temperature of the support maintained during spray deposition (T_{dep}) on the characteristics of the resulting $AgBiS_2$ films was undertaken. The use of T_{dep} below 125 °C did not allow for complete transformation of the precursor to the target material, while excessively hot surface (T_{dep} > 200 °C) promoted formation of unknown phases, presumably silver and/or bismuth oxide-based, in addition to $AgBiS_2$ (*grey* curve in Figure 2a).

Within the optimal 125–225 °C range, the mean crystallite size (estimated for (111), (200) and (220) peaks by applying Scherrer equation with a shape factor of 0.94) gradually increased with temperature from 11 nm at 125 °C to 29 nm at 225 °C (Figure 2a). The highest intensity of the diffraction peaks and therefore the highest degree of crystallinity was achieved at 150 °C. Spray-deposition of the material at higher temperatures also resulted in notable deviation of the relative intensities of the (111) and (200) reflections from the tabulated data for the $AgBiS_2$ cubic phase (Figure 2a), which was ascribed to slight distortion of the crystal structure at T_{dep} > 150 °C.

The surface composition of the spray-deposited $AgBiS_2$ films was determined by XPS, and the results are summarised in Figure 2b-c and Figure S5. The only elements detected at the surface were silver, bismuth, sulphur, oxygen and carbon. The presence of C and O is not unexpected. Most likely it is at least in part due to the products of decomposition of the $AgBiL^Y_2$ precursor, which would be consistent with the observed decrease in the concentration of C with an increase in the spray-deposition temperature (Figure 2c). It is also very common to detect adventitious carbon contamination (incorporating carbon-oxygen functional groups) on any surface by XPS. For the materials obtained at T_{dep} = 125 and 150 °C, the binding energy of the Bi $4f_{7/2}$ peak (158.5 eV) is higher than the value corresponding to elemental Bi (156.9 eV), and is close to reference values for Bi_2S_3 (158.8 eV, see NIST XPS BE database). Binding energy values measured for Ag $3d_{5/2}$ (368.0 eV) and S $2p_{3/2}$ (161.3 eV), while not being unambiguous, are consistent with the Ag-S bonding. The binding energy of S 2s was found to have a consistent value of 225.7 eV. No evidence was detected for the presence of oxidised sulphur species at higher binding energy. At higher spray-deposition temperature of 175 °C, the Ag 3d peak displayed a shift to lower binding energy by about 0.2 eV, and a strong higher binding energy shoulder was observed in the case of the Bi 4f doublet. Both observations suggest the formation of Ag- and Bi-oxides (note that silver represents an exception amongst metals: oxidised species display a negative binding energy shift compared to the metal). The presence of metal oxides at T_{dep} = 175 °C was confirmed by the appearance of a strong O 1s peak at approximately 530 eV (Figure S5b). Importantly, the stoichiometric Ag : Bi ratio of 1 : 1 is achieved for the films deposited at 150 °C, while lower and higher deposition temperatures promote segregation of bismuth and silver, respectively (Figure 2c).

The morphology of the $AgBiS_2$ films deposited at different T_{dep} was studied by SEM. Again, the deposition temperature of 150 °C provided the best results, which in the given context are reflected by very dense and uniform packing of the particles with very low number of pin holes (essentially unidentifiable by

SEM), as can be seen in both top- and side-view images in Figure 3 (top-view micrographs of the underlying ZnO support are provided in Figure S6 for comparison). The lowest number of deposition cycles needed to achieve such quality of the coverage of the support surface with the material was 12. The use of T_{dep} lower or higher than 150 °C (keeping the number of deposition cycles unchanged) deteriorated the quality of the coatings resulting in high concentration of voids or formation of crude segregated agglomerates, respectively. Thickness of the $AgBiS_2$ films deposited under employed conditions with T_{dep} = 150 and 175 °C was uniform within the 60–70 nm range with only slight fluctuations across several-micron-wide side-view SEM images (Figure 3b). Further precise increase in the thickness is possible *via* successive spray depositions under identical conditions. In contrast, coatings deposited at 125 °C exhibited highly variable profiles with thickness ranging from 0 to 120 nm.

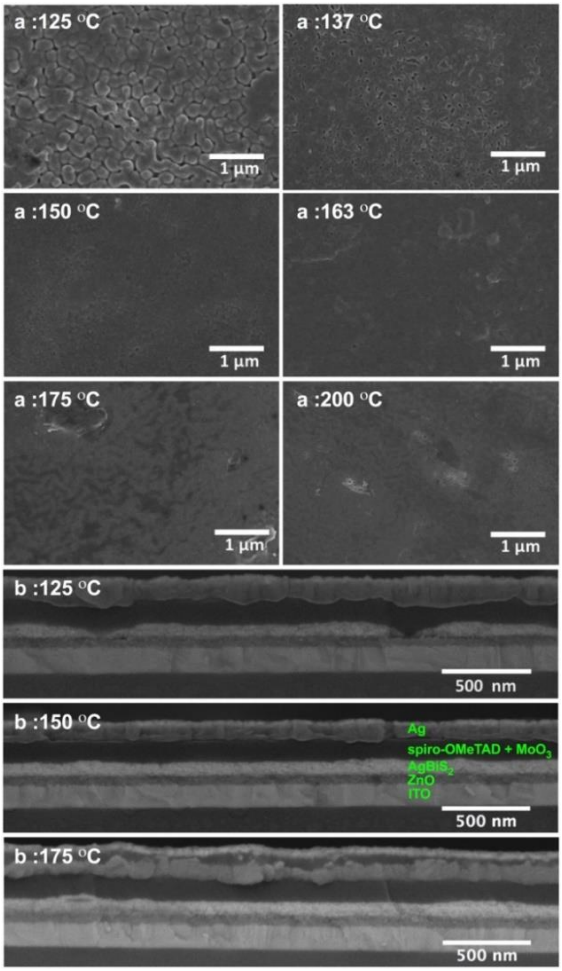

Figure 3. SEM data: (a) top-view images of the $AgBiS_2$ films deposited by spray-pyrolysis onto ZnO|ITO supports at different temperatures, and (b) cross-sectional micrographs of the Ag|MoO_3+spiro-OMeTAD|$AgBiS_2$|ZnO|ITO solar cells with the $AgBiS_2$ light-absorber layers spray-deposited at different T_{dep}.

$AgBiS_2$ films produced by spray-pyrolysis exhibited very broad UV-Vis-NIR absorbance with a cut-off edge at approximately 1100 nm (Figure 4a). It is important to note that recording UV-Vis-NIR spectra of the examined samples in transmission mode only would produce misleading results with apparent significant absorption at wavelengths above 1100 nm (Figure S7). The underlying reason is notable reflectance of the films (Figure S7a), which was measured herein along with transmittance and used to produce the spectra provided in Figure 4a. When analysed in the $(\alpha h\nu)^n - h\nu$ coordinates, the absorption spectra adopt the Tauc pattern for n = ½, which suggests indirect allowed transition.[43] Bandgap values (E_g) estimated by extrapolating linear regions of these plots to zero were essentially independent of the deposition temperature and were close to 1.25 eV.

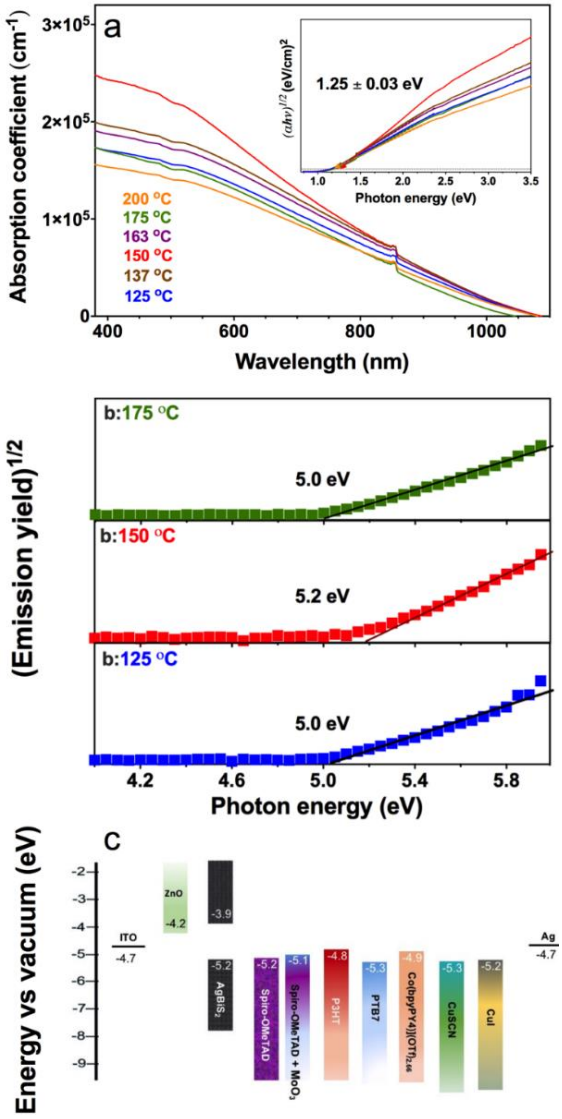

Figure 4. (a) UV-Vis spectra with Tauc plots (inset) and **(b)** PESA data obtained for the $AgBiS_2$ films spray-deposited onto glass at different temperatures: *blue* – 125 °C; *brown* – 137 °C; *red* – 150 °C; *vine* – 163 °C; *green* – 175 °C; *orange* – 200 °C. Panel **(c)** shows energy level diagram for the solar cell components employed herein; data for [Co(bpyPY4)](OTf)$_{2.66}$, CuSCN, CuI, P3HT, PTB7, ITO, ZnO and Ag were taken from literature.[40, 44, 45, 8, 19]

The valence band edge (E_{VB}) measured by photoelectron spectroscopy in air (Figure 4b and Figure S8) and ultraviolet photoelectron spectroscopy (Figure S9, Table S1) varied slightly

within a 0.1 eV range depending on T_{dep}, with the deepest level of *ca* −5.2 eV found for the films obtained at 150 °C. Both E_g and E_{VB} values found here were similar to those reported recently for dense thin layers of $AgBiS_2$ particles.[19] However, it is noted that the spray-deposited material exhibits slightly narrower bandgap (1.25 *vs.* 1.30 eV) and lower energy of the valence band edge (−5.2 *vs*. −5.1 eV), the latter providing slight advantages from the perspective of integration with hole transporters in photovoltaic devices.

Overall, structure and morphology of the silver bismuth sulphide films obtained *via* spray pyrolysis of the $AgBiL^Y_2$ precursor based on methylbenzodithiolate and octanethiol ligands were found to be highly sensitive to the temperature of the support. Notwithstanding such a delicate susceptibility to T_{dep}, the spray deposition procedure was found to be highly reproducible with the highest-quality of the coatings always achieved at 150 °C, which was further mirrored in their photovoltaic properties (*vide infra*). At the same time, temperature maintained during deposition did not significantly affect the optoelectronic properties of the $AgBiS_2$ films.

Deposition and characterisation of Cu_3BiS_3 films

Following the same spray deposition strategy and using a precursor mixture containing bismuth *tris*(4-methylbenzodithioate) with copper(I) acetate and 1,2-ethane dithiol, thin layers of orthorhombic Cu_3BiS_3 can be fabricated on glass or ZnO|ITO supports maintained at 150 °C ≤ T_{dep} ≤ 200 °C as inferred from the XRD data (Figure 5a). Deposition at temperatures above 200 °C promoted formation of unknown phases in addition to Cu_3BiS_3 (Figure 5a), similarly to the results obtained for silver bismuth sulphide layers (Figure 2a). Complete conversion of the precursor to Cu_3BiS_3 was not possible with T_{dep} below 150 °C.

The best quality copper(I) bismuth sulphide films with negligible amount of pinholes (undetectable by SEM as exemplified in Figure 5b) was achieved when the precursor solution was sprayed over the support maintained at 175−200 °C. Thickness of films obtained at these T_{dep} was highly reproducible within the range 70−80 nm when using 12 deposition cycles, which was required for uniform coverage (Figure 5c). Importantly, the quality of the Cu_3BiS_3 films in terms of homogeneity and thickness reported here is significantly better than that of any reported before.[31, 33, 35, 46] Indeed, the finest thin film layers of this material fabricated by spray deposition or evaporation technique were well above 200 nm in thickness and contained coarse (>50 nm), not densely packed Cu_3BiS_3 aggregates (see SEM data in Refs.[32, 33]).

Spray deposited thin films of copper(I) bismuth sulphide exhibited broad light absorption up to *ca* 1000 nm (Figure 5d). Reflectance of these films was notably lower than that of the $AgBiS_2$ samples examined herein (Figure S7 b), but was still considered. Analysis of the UV-Vis data in the $(\alpha h\nu)^n - h\nu$ coordinates does not demonstrate a well-defined linear region which prevents reliable determination of the bandgap (approximation for n = ½ is exemplified in Figure 5d).

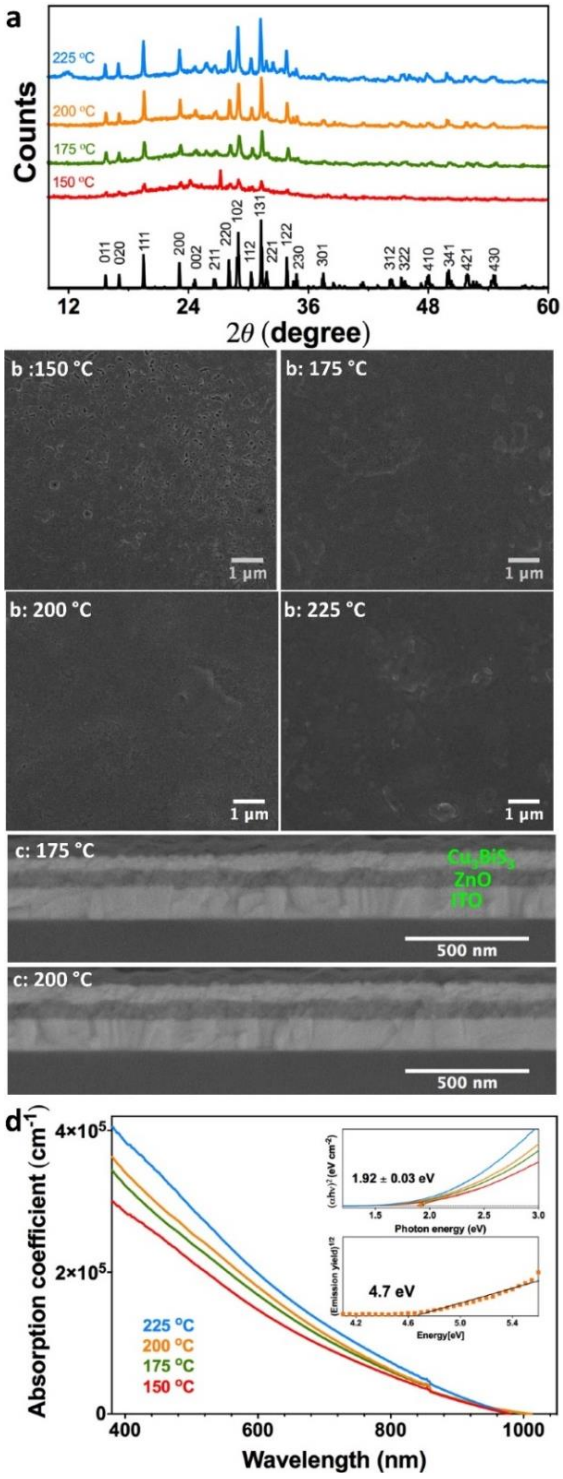

Figure 5. (a) XRD patterns of the Cu_3BiS_3 films formed by spray pyrolysis on a flat glass support at different temperatures: *red* – 150 °C; *green* – 175 °C; *orange* – 200 °C; *blue* – 225 °C. *Black* lines in panel **a** show reference reflections for orthorhombic Cu_3BiS_3 (JCPDS Card File No. 043-1479). (b) Top- and (c) side-view SEM images of the Cu_3BiS_3 films deposited by spray pyrolysis onto ZnO|ITO supports at different temperatures. (d) UV-Vis with Tauc plots (top inset) and PESA data (bottom inset) obtained for the Cu_3BiS_3 films spray deposited onto flat glass supports at different temperatures.

Valence band edge of spray-deposited Cu_3BiS_3 was determined by PESA as *ca* −4.7 eV (Figure 5d), which is consistent with the data reported previously for this material obtained using

different methods.[22, 32] From the perspective of application as a light-absorber in a photovoltaic device, Cu_3BiS_3 would require a hole-transporting material (HTM) with E_{VB} (or highest occupied molecular orbital energy level, HOMO) more positive than −4.7 eV, which is currently unavailable to us. Attempts to use HTMs listed in Figure 4c or no HTM for solar cells based on thin spray-deposited Cu_3BiS_3 layers expectedly produced non-functioning devices. On this basis, photovoltaic performance of the produced material was not assessed herein.

Photovoltaic performance of spray-deposited $AgBiS_2$

Energy levels of major components of planar Ag|HTM|$AgBiS_2$|ZnO|ITO solar cells are summarised in Figure 4c. The choice of ZnO over TiO_2 as an electron transporting material was motivated by a recent promising report on the $AgBiS_2$-based solar cells,[19] as well as general considerations of higher electron mobility.[47] Moreover, initial optimisation experiments undertaken here demonstrated worse results obtained with TiO_2 as compared to ZnO when using a spray pyrolysis method for depositing the $AgBiS_2$ light-absorber.

Comparatively positive valence band edge of silver bismuth sulphide, *viz.* −5.2 - −5.1 eV, requires an appropriate hole-transporting material to have a HOMO/E_{VB} edge above this energy level. Theoretically, HTMs not complying with this requirement should not allow for any reasonable photon to current conversion efficiency. However, and surprisingly, this was not the case in the work of Bernechea *et al.*[19] who achieved the best results for their $AgBiS_2$-based devices, *viz.* power conversion efficiency (PCE) of 4.8 ± 0.4%, when using PTB7 with the HOMO level of −5.3 eV. Slightly worse, though still reasonable PCEs of 3.3 and 1.2% were reported in their work for solar cells employing PCE-10 (HOMO at −5.4 eV) and spiro-OMeTAD (HOMO at −5.2 eV), respectively. Interestingly, a HTM that provides proper energy alignment with $AgBiS_2$, *viz.* P3HT having HOMO at −4.8 eV, allowed for lower performance (PCE 3.9 %) as compared to PTB7 in the work of Bernechea *et al.*[19] It should be noted that these results were obtained with HTM layers that were additionally modified with evaporated MoO_3, which might influence the electronic characteristics of hole transporters.[48] We were able to successfully reproduce the above results from Ref.[19] when using MoO_3-modified spiro-OMeTAD and P3HT as HTMs, but unexpectedly, failed to achieve reasonable performance with PTB7 notwithstanding significant number of attempts undertaken (Figure S10, Table S2). Rationalisation of the latter result requires further investigations that go beyond the scope of the present work.

Herein, we also examined a range of compounds as hole-transporting materials in the planar photovoltaic devices based on spray-deposited $AgBiS_2$, which included PTB7 (HOMO −5.3 eV),[19] CuSCN (E_{VB} −5.3 eV),[45] CuI (E_{VB} −5.2 eV),[44] spiro-OMeTAD (HOMO −5.2 eV, as reported elsewhere[49] and confirmed here by UPS), $[Co(bpyPY4)](OTf)_{2.66}$ (HOMO −4.9 eV)[40] and P3HT (HOMO −4.8 eV)[19] (Figure 11, Table S3). The effect of MoO_3 evaporated onto pre-deposited organic HTM layers was also considered. The performance of the Ag|HTM|$AgBiS_2$|ZnO|ITO solar cells with different HTMs is summarised in Table S3.

Devices with no hole transporting layer did not generate any measurable photocurrent. The photovoltaic performance achieved with inorganic HTMs and $[Co(bpyPY4)](OTf)_{2.66}$ was also very poor: PCE 0.20 ± 0.04 % for CuSCN and PCE < 0.1 % for CuI and cobalt complex. The latter result was to some extent unexpected, as alignment of the HOMO energy level of this hole-transporter (−4.9 eV) and E_{VB} of the light-absorber (−5.2 eV) was highly favourable. Similarly well-aligned P3HT also provided low open-circuit voltage (V_{oc}) of 227 mV and PCE of only 0.43 % with spray-deposited silver bismuth disulphide, and no improvements were possible by introducing evaporated MoO_3 or common HTM additives like lithium bis(trifluoromethanesulfonyl)imide (LiTFSI) and tert-butylpyridine (tBP). This finding was again unexpected given that P3HT was confirmed here to allow for reasonable efficiency of the $AgBiS_2$-based solar cells fabricated following the strategy devised by Bernechea *et al.*[19] (Figure S10, Table S2). Moreover, the quality of the films obtained by the procedure from Ref.[19] was not better than that achieved *via* spray pyrolysis of $AgBiL^Y_2$ (*cf.* Figure S10a and Figure 3, T_{dep} = 150 °C). This observation suggests that other factors than short-circuiting through pin holes in a thin light-absorber film produced by the latter method contributed to the poor photovoltaic performance with P3HT as a hole transporter (Figure S11 and Table S3). Unsatisfactory results were obtained when PTB7 was used as a HTM in the planar solar cells based on the spray-deposited $AgBiS_2$ thin films, which was rationalised in terms of improper alignment of the energy levels (Figure 4c).

Among all HTMs examined, only partially oxidised spiro-OMeTAD sustained reasonable photovoltaic efficiency of the solar cells based on $AgBiS_2$ obtained *via* spray pyrolysis (Table S3), and therefore detailed investigation of the devices with this configuration was undertaken. Examples of the photocurrent density (*J*) *vs.* voltage (*V*) curves, quasi-steady-state PCE transients and incident photon-to-current conversion efficiency (IPCE) spectra of the devices are provided in Figure 6a, b and c, while major photovoltaic parameters derived from these data are summarised in Figure 6d and Table S4. All examined cells exhibited small (Figure 6a) or essentially no hysteresis (Table S4) during *J-V* measurements under employed conditions. Photovoltaic performance was also stable during short-term chronoamperometric measurements at the voltage corresponding to the maximum power point in the voltammetric curves (Figure 6b).

Modification of the HTM layer with MoO_3 significantly enhanced short circuit current density (J_{sc}) and open-circuit voltage of the $AgBiS_2$-based solar cells examined here (Figure 6d). Moreover, introduction of MoO_3 decreased the series resistance and increased the shunt resistance of the devices as inferred from the *J-V* data (exemplified in Figure S12 and Table S5). According to the literature,[50] MoO_3 minimises recombination, interfacial power losses and enhances the carrier mobility rate. Notably, PESA measurements undertaken here suggest that depositing MoO_3 over spiro-OMeTAD upshifts the HOMO level of the HTM material by 0.1 eV (Figure 4c), which might facilitate hole extraction and thereby improve the photovoltaic efficiency. The possibility for evaporated MoO_3 to

penetrate into charge-transporting layers and thereby alter their electronic properties was reported previously.[48]

Figure 6c, d and Table S4 summarise the effect of temperature used for spray deposition of the $AgBiS_2$ light absorber on the photovoltaic performance of the Ag|MoO_3+spiro-OMeTAD|$AgBiS_2$|ZnO|ITO solar cells. The highest IPCE, power conversion efficiency, short-circuit current density and open-circuit voltage were achieved with T_{dep} = 150 °C, which is consistent with the outcomes of the physical characterisation. Indeed, the best-quality films (Figure 3), the highest degree of crystallinity of undistorted and pure cubic $AgBiS_2$ (Figure 2a), appropriate surface stoichiometry (Figure 2c), and slightly improved optoelectronic characteristics (Figure 4) were all achieved at this temperature. Decreased series resistance at T_{dep} = 150 °C as compared to those fabricated at 125 or 175 °C (Table S5) reflects better charge separation leading to higher short circuit current. It is reasonable to suggest that recombination of photogenerated charges in the examined films should depend on concentration of defects that changes with T_{dep} and affects the current generation and quantum efficiency (Figure 6c and Table S4). Fill factor improved negligibly with an increase in T_{dep} (Figure 6d, Table S4), but significantly lower series resistance was provided by deposition temperature of 150 °C (Table S5), which can be interpreted in terms of improved electrical contact between $AgBiS_2$ and charge-transporting layers.

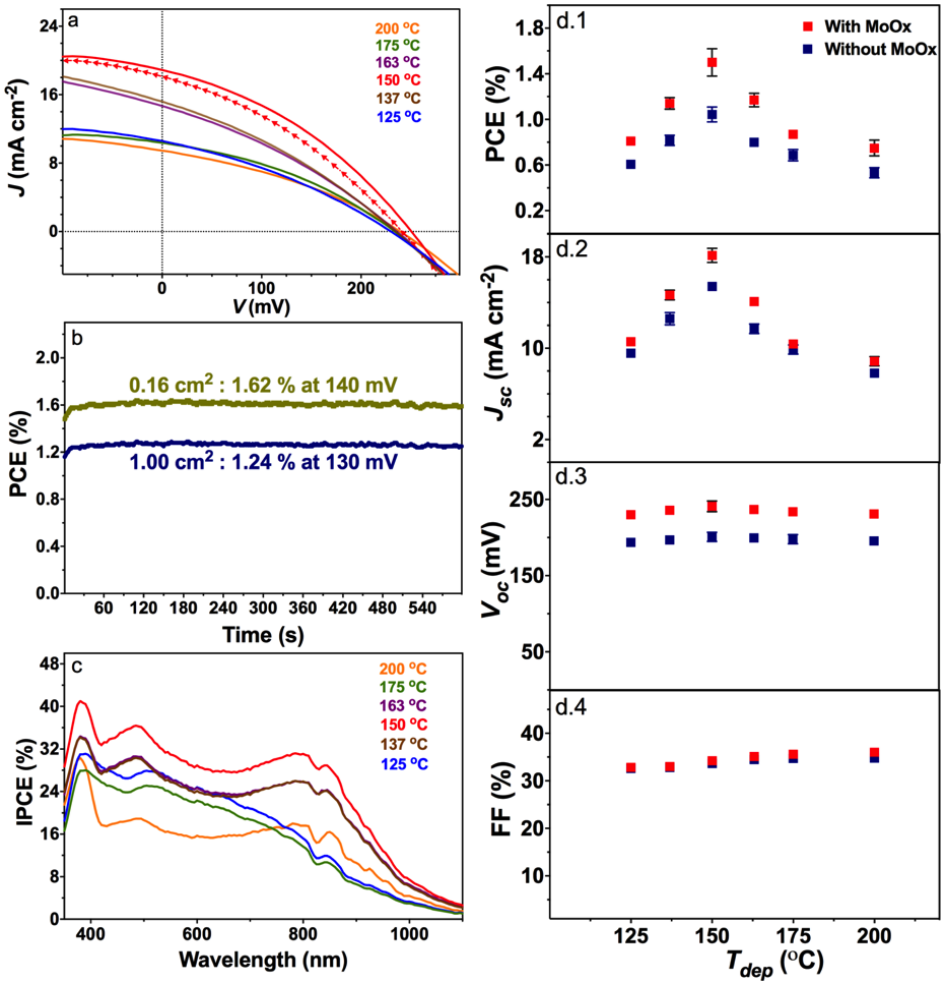

Figure 6. Photovoltaic performance of the Ag|MoO_3+spiro-OMeTAD|$AgBiS_2$|ZnO|ITO solar cells (aperture 0.16 cm^2) with the light-absorber layer spray-deposited at different temperatures: (a) photocurrent density *vs.* voltage curves (sweep rate 100 mV s^{-1}; scans in both directions are shown for 150 °C, but only short-circuit to open-circuit sweeps are provided in other cases) under 1 sun AM 1.5 G irradiation (dotted lines are guides to the eye showing zero *J* and *V*); (b) quasi-steady-state power output for the devices tested with an aperture of 0.16 (*tan*) and 1 cm^2 (*navy*) under 1 sun AM1.5G irradiation; (c) IPCE spectra. (d) Dependence of (d.1) PCE (power conversion efficiency), (d.2) J_{sc} (short circuit current density), (d.3) V_{oc} (open circuit voltage). and (d.4) FF (fill factor) of the devices with (*red*) and without MoO_3 (*blue*) on the $AgBiS_2$ deposition temperature; mean values and one standard deviation for 10 independent solar cells are shown (data were derived from *J-V* curves as in panel **a** measured from short-circuit to open-circuit).

Solar cells in Figure 6 demonstrated very promising short-circuit current density, but their open-circuit voltage and fill factor were comparatively low. These devices were fabricated with the number of $AgBiS_2$ spray deposition cycles of 12, which produced 60-70 nm thick chalcogenide layers at T_{dep} = 150 °C for the best-performing cells. Notwithstanding the SEM evidence for the very high quality of the spray-deposited films obtained under the optimised conditions at 150 °C (Figure 3), we

hypothesised that voids in these thin $AgBiS_2$ layers might be still present and contribute to low V_{oc} and FF. Indeed, investigation of the effect of the number of deposition cycles on the photovoltaic performance circumstantially confirmed the above supposition, as summarised in Figure S13 and Table S6. Open-circuit voltage and fill factor enhanced from 187 ± 6 mV to 434 ± 4 mV and from 32.2 ± 0.4 to 42.1 ± 0.4, respectively, when the number of spray cycles was increased from 10 to 18. Unfortunately, the short-circuit current density did not follow the same trend, but peaked at 12 cycles and abruptly degraded for thicker films. Most probably, short charge diffusion length in $AgBiS_2$[16] is the major cause for reduced short circuit current density in thicker films. Significant recombination of the photogenerated charge carriers in the examined $AgBiS_2$-based devices is supported by not strictly linear dependence of the short-circuit current density on the illumination intensity (P), $J_{sc} \propto P^{0.95}$ (Figure S14a). An ideality factor of 1.5 derived from the dependence of V_{oc} on P (Figure S14b) indicates trap-assisted recombination, which could be probably due to the pin holes in the film and possible surface defects leading to notable reduction in the open circuit voltage.

Thus, the best photovoltaic performance under 1 sun irradiation was achieved here with the $AgBiS_2$ layers deposited at 150 °C with the thickness of 60–70 nm and MoO_3+spiro-OMeTAD as a hole-transporter. These devices exhibit a short-circuit current density of 18.1 ± 0.6 mA cm^{-2}, which is higher than that reported previously for the $AgBiS_2$ cells featuring MoO_3+spiro-OMeTAD HTM layers (6.6 mA cm^{-2}).[19] In principle, higher thickness of the $AgBiS_2$ light absorber layer in our devices (60–70 nm *vs.* approximately 40 nm in Ref.[19]) might be a plausible reason for this improvement, although the data reported by Bernechea *et al.*[19] and our results (Table S5) suggest that this difference cannot produce such large enhancement in photocurrent. One can also hypothesise that higher J_{sc} might be due to denser packing of the $AgBiS_2$ crystallites within the films and overall improved homogeneity thereof provided by the spray deposition technique, but we acknowledge that no solid confirmation of this supposition is currently available. Moreover, notably lower V_{oc} achieved with our method along with other evidence presented above suggests that recombination and short-circuiting in the devices based on the spray-deposited $AgBiS_2$ is more pronounced than in the previous report.[19] Given that fill factor of the solar cells examined here was also lower, one might also suggest that charge transfer across the interfaces between the light absorber and charge selective materials requires thorough optimisation. Passivation of the surface of $AgBiS_2$ with tetramethylammonium iodide[19] did not improve the performance of our devices. Obviously, other strategies need to be established to allow for facilitated charge injection from $AgBiS_2$ into hole- and electron-transporting materials.

Nevertheless, the power conversion efficiencies of the Ag|MoO_3+spiro-OMeTAD|$AgBiS_2$|ZnO|ITO solar cells based on spray-deposited silver bismuth sulphide reached 1.7 and 1.2 % when tested with an aperture of 0.16 and 1.00 cm^2, respectively (Figure 6 and Table S4). This is better performance than 1.2 % measured with an aperture of 0.16 cm^2 for the devices where the light-absorber was deposited by spin coating the dispersion of pre-formed oleate-capped nanoparticles (Figure S10). Finally, non-encapsulated devices with $AgBiS_2$ layers produced by spray deposition and MoO_3+spiro-OMeTAD as a HTM exhibited essentially no degradation when stored for 1 month under diffuse light under ambient conditions at approximately 50 % relative humidity and 24 ± 2 °C. Indeed, all major photovoltaic parameters only slightly varied over the examined period as shown in Figure S15.

Conclusion

Low-temperature spray pyrolysis of bismuth(III) *tris*(4-methylbenzodithioate) solutions containing a relevant first group metal precursor enables deposition of <100 nm thick films of α cubic rock salt $AgBiS_2$ and orthorhombic Cu_3BiS_3 onto flat supports at temperatures not higher than 200 °C on air. The deposition conditions were optimised here to produce homogeneous and densely packed films of 10–20 nm crystallites of the above ternary chalcogenides with the uniform thickness as low as 60–70 nm. Deposition temperature was identified as a key parameter determining the morphology, structure, and to a much lower extent, optoelectronic properties of the resulting materials. Integration of the spray-deposited $AgBiS_2$ films with a ZnO electron transporting layer and MoO_3-modified spiro-OMeTAD hole transporting material produces thin planar solar cells with an average power conversion efficiency of 1.5 ± 0.1 % that are stable under ambient conditions for at least 1 month. These devices exhibit high short-circuit current density of 18.1 ± 0.6 mA cm^{-2} under 1 sun irradiation, which is a notable improvement over previous reports on the $AgBiS_2$-based photovoltaic cells. However, the overall performance is limited by lower than expected open-circuit voltage and fill factor, which might be associated with short-circuiting through very small pinholes in thin spray-deposited $AgBiS_2$ layers, although we could not identify this morphological imperfection in the produced films using SEM. Notable improvement in V_{oc} up to *ca* 400 mV is possible with an increase in the thickness of $AgBiS_2$, though it comes at the expense of the photocurrent density. Future studies to explore injection mechanisms and to understand the effects of surface passivation and structural defects are needed for the design of better performing devices with suppressed recombination and facilitated charge transfer between chalcogenide light-harvester and charge-selective transporting layers.

In summary, the low-temperature, solution-based and highly reproducible method reported in the present work offers a new versatile strategy for fabrication of ternary chalcogenide thin films for various applications. Another critical advantage of the developed method is straightforward scalability. Herein, fabrication of thin $AgBiS_2$ and Cu_3BiS_3 films with the dimensions of 2.5 cm × 2.5 cm is demonstrated, as is a functioning 1 cm^2 $AgBiS_2$-based photovoltaic device. The only requirement for spray coating of larger surfaces is uniform heating of the support.

Conflicts of interest

There are no conflicts to declare.

Acknowledgements

The authors are grateful to Dr. I. Benesperi for the synthesis of Co(bpyPY4)](OTf)$_{2.66}$, and acknowledge the Australian Centre for Advanced Photovoltaics (ACAP), the Australian Renewable Energy Agency and the Australian Research Council for their financial support through the ARC Centre of Excellence in Exciton Science (CE170100026), ARC Centre of Excellence for Electromaterials Science (CE140100012) and a discovery project (DP160104575). Electron microscopy access provided by the Monash University Centre for Electron Microscopy (MCEM) is greatly acknowledged.

Notes

$^{\perp}$To the inexpressible sorrow of the co-authors, Prof. Leone Spiccia has passed away untimely before this work could be published.

References

1. D. Aldakov, A. Lefrançois and P. Reiss, *Journal of Materials Chemistry C*, 2013, **1**, 3756-3776.
2. G. Tan, L.-D. Zhao and M. G. Kanatzidis, *Chemical Reviews*, 2016, **116**, 12123-12149.
3. S. Anantharaj, S. Ede, K. Sakthikumar, K. Karthick, S. Mishra and S. Kundu, *ACS Catalysis*, 2016, 6, 8069−8097.
4. F.-J. Fan, L. Wu and S.-H. Yu, *Energy Environ Sci*, 2013, **7**, 190-208.
5. I. Chung and M. G. Kanatzidis, *Chemistry of Materials*, 2014, **26**, 849-869.
6. J. Mal, Y. V. Nancharaiah, E. D. van Hullebusch and P. N. L. Lens, *RSC Advances*, 2016, **6**, 41477-41495.
7. V. Lakshmi, Y. Chen, A. A. Mikhaylov, A. G. Medvedev, I. Sultana, M. Rahman, O. Lev, P. Prikhodchenko and A. M. Glushenkov, *Chemical Communications*, 2017, DOI: 10.1039/C7CC03998K.
8. M.-R. Gao, Y.-F. Xu, J. Jiang and S.-H. Yu, *Chemical Society Reviews*, 2013, **42**, 2986-3017.
9. M. Chatti, T. Gengenbach, R. King, L. Spiccia and A. N. Simonov, *Chem. Mater.*, 2017, DOI: 10.1021/acs.chemmater.7b00114.
10. M. Osborne, First Solar pushes CdTe cell efficiency to record 22.1%, (accessed 23-02-2016, 2016).
11. G. H. Carey, A. L. Abdelhady, Z. Ning, S. M. Thon, O. M. Bakr and E. H. Sargent, *Chemical Reviews*, 2015, **115**, 12732-12763.
12. M. G. Panthani, M. J. Kurley, R. W. Crisp, T. C. Dietz, T. Ezzyat, J. M. Luther and D. V. Talapin, *Nano letters*, 2014, **14**.
13. G. Chen, J. Seo, C. Yang and P. N. Prasad, *Chem. Soc. Rev.*, 2013, **42**, 8304-8338.
14. C. Yan, E. Gu, F. Liu, Y. Lai, J. Li and Y. Liu, *Nanoscale*, 2013, **5**, 1789-1792.
15. S. N. Guin and K. Biswas, *Chemistry of Materials*, 2013, **25**, 3225-3231.
16. B. Pejova, D. Nesheva, Z. Aneva and A. Petrova, *J. Phys. Chem. C*, 2011, **115**, 37-46.
17. N. Liang, W. Chen, F. Dai, X. Wu, W. Zhang, Z. Li, J. Shen, S. Huang, Q. He, JiantaoZai, N. Fang and X. Qian, *CrystEngComm*, 2015, **17**, 1902-1905.
18. P.-C. Huang, W.-C. Yang and M.-W. Lee, *The Journal of Physical Chemistry C*, 2013, **117**.
19. M. Bernechea, N. Miller, G. Xercavins, D. So, A. Stavrinadis and G. Konstantatos, *Nat. Photon.*, 2016, **10**, 521-525.
20. C. Chen, X. Qiu, S. Ji, C. Jia and C. Ye, *CrystEngComm*, 2013, **15**, 7644-7648.
21. F. Viñes, M. Bernechea, G. Konstantatos and F. Illas, *Phys. Rev. B*, 2016, **94**.
22. J. Yin and J. Jia, *CrystEngComm*, 2013, **16**, 2795-2801.
23. N. Wang, *Mineralogical Magazine*, 1994, **58**, 201-204.
24. S. Geller, *Acta Crystallogr.*, 1959, **12**.
25. D. Chen, G. Shen, K. Tang, X. Jiang, L. Huang, Y. Jin and Y. Qian, *Inorganic Chemistry Communications*, 2003, **6**, 710-712.
26. G. Shen, D. Chen, K. Tang and Y. Qian, *Journal of Crystal Growth*, 2003, **252**, 199-201.
27. T. Thongtem, N. Tipcompor and S. Thongtem, *Materials Letters*, 2010, **64**, 755-758.
28. T. Thongtem, J. Jaroenchaichana and S. Thongtem, *Materials Letters*, 2009, **63**, 2163-2166.
29. D. Liu, D. Cai, Y. Yang, H. Zhong, Y. Zhao, Y. Song, S. Yang and H. Wu, *Applied Surface Science*, 2016, **366**, 30-37.
30. J. Zhong, W. Xiang, C. Xie, X. Liang and X. Xu, *Mater. Chem. Phys.*, 2013, **138**, 773-779.
31. N. J. Gerein and J. A. Haber, *Chem. Mater.*, 2006, **18**, 6289-6296.
32. A. Hussain, R. Ahmed, N. Ali, N. M. AbdEl-Salam, K. bin Deraman and Y. Fu, *Surf. Coat. Technol.*, 2017, **320**, 404-408.
33. S. Liu, X. Wang, L. Nie, L. Chen and R. Yuan, *Thin Solid Films*, 2015, **585**, 72-75.
34. L. Zhang, X. Jin, C. Yuan, G. Jiang, W. Liu and C. Zhu, *Appl. Surf. Sci.*, 2016, **389**, 858-864.
35. S. G. Deshmukh, A. K. Panchal and K. Vipul, *Chemical bath deposition of Cu3BiS3 thin films*, 2016, DOI: 10.1063/1.4946073, 20023.
36. D. C. Senevirathna, M. V. Werrett, N. Pai, V. L. Blair, L. Spiccia and P. C. Andrews, *Chemistry - A European Journal*, 2017, DOI: 10.1002/chem.201701952.
37. B. Pejova, I. Grozdanov, D. Nesheva and A. Petrova, *Chem. Mater.*, 2008, **20**, 2551-2565.
38. A. M. S. Ibrahim, Laila I, *Fizika A*, 1996, **5**, 177-184.
39. T. G. Deepak, G. S. Anjusree, N. K. R. Pai, D. Subash, S. V. Nair and S. A. Nair, *RSC Advances*, 2014, **4**, 23299-23303.
40. M. K. Kashif, R. A. Milhuisen, M. Nippe, J. Hellerstedt, D. Z. Zee, N. W. Duffy, B. Halstead, F. Angelis, S. Fantacci, M. S. Fuhrer, C. J. Chang, Y. B. Cheng, J. R. Long, L. Spiccia and U. Bach, *Advanced Energy Materials*, 2016, **6**, 1600874.
41. D. C. Senevirathna, V. L. Blair, M. V. Werrett and P. C. Andrews, *Dalton Trans.*, 2016, **45**, 4998-5000.
42. A. S. Hassanien and A. A. Akl, *Superlattices and Microstructures*, 2016, **89**, 153-169.
43. B. D. Viezbicke, S. Patel, B. E. Davis and D. P. Birnie, *physica status solidi (b)*, 2015, **252**, 1700-1710.
44. G. A. Sepalage, S. Meyer, A. Pascoe, A. D. Scully, F. Huang, U. Bach, Y. B. Cheng and L. Spiccia, *Adv. Funct. Mater.*, 2015, **25**, 5650-5661.
45. G. A. Sepalage, S. Meyer, A. R. Pascoe, A. D. Scully, U. Bach, Y.-B. Cheng and L. Spiccia, *Nano Energy*, 2017, **32**, 310-319.
46. S. G. Deshmukh, S. J. Patel, K. K. Patel, A. K. Panchal and V. Kheraj, *J. Electron. Mater.*, 2017, DOI: 10.1007/s11664-017-5642-2, 1-7.
47. Q. Zhang, C. S. Dandeneau, X. Zhou and G. Cao, *Adv. Mater.*, 2009, **21**, 4087-4108.
48. R. T. White, E. S. Thibau and Z.-H. Lu, *Scientific Reports*, 2016, **6**, 21109.

49. U. B. Cappel, T. Daeneke and U. Bach, *Nano Lett.*, 2012, **12**, 4925-4931.
50. I. Hancox, K. V. Chauhan, P. Sullivan, R. A. Hatton, A. Moshar, C. P. A. Mulcahy and T. S. Jones, *Energy Environ Sci*, 2009, **3**, 107-110.